Trapped Ion Quantum Computing Using Optical Tweezers and Electric Fields

M. Mazzanti,[1] R. X. Schüssler,[1] J. D. Arias Espinoza,[1] Z. Wu,[1] R. Gerritsma,[1,2] and A. Safavi-Naini[2,3]
[1]Van der Waals–Zeeman Institute, Institute of Physics, University of Amsterdam, 1098 XH Amsterdam, Netherlands
[2]QuSoft, Science Park 123, 1098 XG Amsterdam, Netherlands
[3]Institute for Theoretical Physics, Institute of Physics, University of Amsterdam, Science Park 904, 1098 XH Amsterdam, Netherlands

(Received 17 June 2021; accepted 9 November 2021; published 22 December 2021)

We propose a new scalable architecture for trapped ion quantum computing that combines optical tweezers delivering qubit state-dependent local potentials with oscillating electric fields. Since the electric field allows for long-range qubit-qubit interactions mediated by the center-of-mass motion of the ion crystal alone, it is inherently scalable to large ion crystals. Furthermore, our proposed scheme does not rely on either ground-state cooling or the Lamb-Dicke approximation. We study the effects of imperfect cooling of the ion crystal, as well as the role of unwanted qubit-motion entanglement, and discuss the prospects of implementing the state-dependent tweezers in the laboratory.

DOI: 10.1103/PhysRevLett.127.260502

Introduction.—Trapped ions form one of the most mature laboratory systems for quantum information processing and quantum simulation [1–3]. Many of the basic building blocks needed for these technologies have been demonstrated: high fidelity detection and preparation [4] and universal quantum operations performed by external fields coupling to the internal states of the ions. While quantum gates have been performed with very high fidelities in trapped ions [5–7], scaling up the system while maintaining the quality of operations has proven to be challenging. In particular, as the length of ion crystals increases, the number of motional modes to which the gate lasers couple also increases. This leads to a reduction of interaction strength for gates between distant qubits [8]. Furthermore, the number of degrees of freedom with which the qubits can erroneously entangle increases.

Here we propose a novel universal trapped ion quantum computing architecture that uses state-dependent optical tweezer potentials [9–11] combined with oscillating electric fields to overcome the obstacles described above. Since the electric fields only couple to the center-of-mass (c.m.) mode of the ion crystal, adverse effects of spectator modes that reduce the range of interaction are avoided. Moreover, our gate does not rely on the Lamb-Dicke approximation, which requires the wave packets of the ions to be confined to a space smaller than the wavelength of the laser implementing the gate. This extends the parameter regime for gate operation. The combination of such 2-qubit gates with single-qubit gates can be used as a universal quantum computer.

We illustrate the gate mechanism applied to qubits i and j in Fig. 1. We simultaneously apply an electric field of amplitude E_0 oscillating close to the c.m. frequency (at detuning δ) and optical tweezers to the two addressed qubits. The gate works as follows: the tweezers shift the frequency of the c.m. mode in a state-dependent manner, such that for two qubits in the same state the electric field can no longer excite motion. Thus, the evolution of the system is dominated by phonon mediated effective spin-spin interactions $\propto E_0^2/\delta$. We perform a geometric phase gate by choosing the appropriate E_0 and δ. Since the interactions are merely mediated by the c.m. mode, they are independent of distance. Additionally, the required tweezer power scales linearly with the number of ions in the crystal. Both those factors contribute to the scalability of our proposal.

Realizing a geometric phase gate.—Consider a crystal of N ions with masses M and charge e in a harmonic trap. The normal modes (phonon modes) and mode frequencies of the crystal can be found by diagonalizing the Hessian

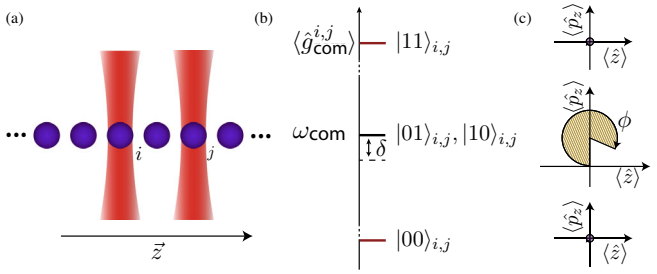

FIG. 1. (a) Schematic representation of a linear chain of ions where optical tweezers are applied to ions i and j. The tweezers shift the c.m. mode depending on the internal state of the pair. (b) Level scheme of the four states; only the states $|01\rangle$ and $|10\rangle$ are unaffected by the extra trapping potential generated by the tweezers. (c) Phase space dynamics of the four states when adding an electric field at a frequency $\omega_{\mathrm{com}} - \delta$. Because of the displacement generated by the driving electric field, the states $|01\rangle$ and $|10\rangle$ acquire a phase ϕ.

matrix $\mathbf{A}$ [12]. Here $A^{(ij)} = d^2V/(d\alpha_i d\alpha_j)$, where α_i are small deviations about the equilibrium positions of the ions, and V is the total potential energy. The eigenvectors of the Hessian, denoted by $\mathbf{b}_m$, are the normal modes of the crystal. The mode frequencies are given by $\omega_m = \sqrt{\lambda_m}$, with λ_m as the eigenvalues of $\mathbf{A}$. For a 1D ion crystal, the eigenmodes separate into three subclasses, corresponding to the directions of motion x, y, z. In the following, we focus on the axial direction (z) characterized by the trap frequency ω_z.

We address a specific ion using tweezers formed by focused beams aligned on its equilibrium position, leaving the geometry of the crystal independent of the qubit states. Moreover, we will show that the laser parameters and qubit states can be chosen such that the dynamical polarizability of the qubit states $|0\rangle$ and $|1\rangle$ are of equal magnitude, but opposite sign. If the ions are confined to the tweezer waist, the tweezer potential can be approximated by a state-dependent harmonic potential: $\hat{H}_{\mathrm{tw}}^{i,j} = \frac{1}{2}M\omega_{\mathrm{tw}}^2(\hat{z}_i^2\hat{\sigma}_z^i + \hat{z}_j^2\hat{\sigma}_z^j)$. Here, $\hat{\sigma}_z^i$ ($\hat{\sigma}_z^j$) is the Pauli matrix operating on ion i (j) and $\hat{z}_i$ ($\hat{z}_j$) is the position operator relative to the equilibrium position of ion i (j). The proposed gate requires the simultaneous application of the tweezers and an oscillating electric field generated by applying a rf voltage to an electrode close to the ion crystal. The total Hamiltonian is then given by

$$\hat{H} = \sum_m \omega_m \left(\hat{a}_m^\dagger \hat{a}_m + \frac{1}{2}\right) + \hat{H}_{\mathrm{tw}}^{i,j} + \hat{H}_E(t), \qquad (1)$$

with $\hat{H}_E(t)$ denoting the electric field interaction and $\hat{a}_m^\dagger$ ($\hat{a}_m$) the creation (annihilation) operator of mode m. Since a homogeneous electric field E_0 only couples to the c.m. motion,

$$\hat{H}_E(t) = 2\gamma(\hat{a}_{\mathrm{com}}^\dagger + \hat{a}_{\mathrm{com}})\cos(\mu t),$$

where $\gamma = eE_0 l_{\mathrm{com}}/2$, $l_{\mathrm{com}} = (2M\omega_{\mathrm{com}})^{-1/2}$, and $\mu = \omega_{\mathrm{com}} + \delta$ is the frequency of the electric field. If $\omega_{\mathrm{tw}} \ll \omega_m$ for all modes, we can use perturbation theory to find the new mode frequencies in the presence of the tweezers: $\tilde{\lambda}_m \approx \lambda_m + \sum_k b_{mk}\hat{A}_{\mathrm{tw}}^{(ij)} b_{mk} + \ldots$, with $k = 1, \ldots, N$. Here, the perturbation of the tweezers to the Hessian matrix is given by $\hat{A}_{\mathrm{tw}}^{(ij)} = \omega_{\mathrm{tw}}^2(\hat{\sigma}_z^i + \hat{\sigma}_z^j)$. To first order,

$$\tilde{\omega}_m^{i,j} \approx \sqrt{\omega_m^2 + \omega_{\mathrm{tw}}^2(b_{mi}^2\hat{\sigma}_z^i + b_{mj}^2\hat{\sigma}_z^j)}, \qquad (2)$$

which shows that the mode frequencies shift depending on the states of qubits i and j.

In order to gain intuition about the dynamics generated by Eq. (1), we apply the unitary transformation $\hat{U}_1 = \exp[i(\delta\hat{a}_{\mathrm{com}}^\dagger\hat{a}_{\mathrm{com}} + \sum_m \omega_m\hat{a}_m^\dagger\hat{a}_m)t]$, as well as the rotating wave approximation, neglecting terms oscillating faster than δ. Next, we apply Lang-Firsov unitary transformation [13], $\hat{U}_2 = \exp[\hat{V}(\hat{a}_{\mathrm{com}}^\dagger - \hat{a}_{\mathrm{com}})]$, with $\hat{V} = \gamma(\hat{g}_{\mathrm{com}}^{i,j} - \delta\mathbb{1})^{-1}$. This eliminates the first-order phonon coupling. The resulting Hamiltonian is

$$\hat{H}_2 = \sum_m \hat{g}_m^{i,j}(\hat{a}_m^\dagger\hat{a}_m + 1/2) - \delta\hat{a}_{\mathrm{com}}^\dagger\hat{a}_{\mathrm{com}} - \frac{\gamma^2}{2\delta}\hat{\sigma}_z^i\hat{\sigma}_z^j + \frac{\gamma^2}{g_{\mathrm{com}}^+ - \delta}\hat{W}_+ + \frac{\gamma^2}{g_{\mathrm{com}}^- - \delta}\hat{W}_-, \qquad (3)$$

with $\hat{W}_+ = |11\rangle_{ij}\langle 11|_{ij}$ and $\hat{W}_- = |00\rangle_{ij}\langle 00|_{ij}$, where we have dropped energy offset terms $\propto \mathbb{1}$. The operator $\hat{g}_m^{i,j} = \tilde{\omega}_m^{i,j} - \omega_m$ contains the qubit-state dependence and $g_{\mathrm{com}}^\pm$ are calculated by setting $\hat{\sigma}_z^i + \hat{\sigma}_z^j \to \pm 2$. For the c.m. mode, $\mathbf{b}_{\mathrm{com},i}^2 = \mathbf{b}_{\mathrm{com},j}^2 = 1/N$ [12], thus $\hat{g}_{\mathrm{com}}^{ij} = \sqrt{\omega_{\mathrm{com}}^2 + \omega_{\mathrm{tw}}^2(\hat{\sigma}_z^{(i)} + \hat{\sigma}_z^{(j)})/N} - \omega_{\mathrm{com}}$ (see Fig. 1). In the limit $\omega_{\mathrm{tw}} \ll \omega_{\mathrm{com}}$, we obtain $\hat{g}_{\mathrm{com}}^{ij} \approx \omega_{\mathrm{tw}}^2(\hat{\sigma}_z^{(i)} + \hat{\sigma}_z^{(j)})/(2N\omega_{\mathrm{com}})$, which shows that for a given $\hat{g}_{\mathrm{com}}^{ij}$ the tweezer intensity should scale linearly with N.

Effective Hamiltonian.—The first line of the Hamiltonian (3) contains the qubit-state dependence of the phonon modes. This may lead to residual qubit-phonon entanglement at the end of the gate, causing errors. However, straightforward spin-echo sequences correct these errors. The second line contains the qubit-qubit interactions, and the first term dominates for $|\delta| \ll |g^\pm|$. To achieve a geometric phase gate, we set the gate time to $\tau = 2\pi/\delta$ and $\gamma^2/\delta^2 = \pi/4$ [14,15].

To characterize the gate under experimental conditions, we first consider two $^{171}\mathrm{Yb}^+$ ions with trap frequency $\omega_{\mathrm{com}} = 2\pi \times 1$ MHz. Next, we consider $N = 4$ ions to demonstrate the scalability of our scheme. We assume that the ions are initialized in a thermal state with $\bar{n}$ motional quanta. The gate sequence consists of four pulses of duration $\tau = 2\pi/\delta$, as illustrated in Fig. 2(a). Each pulse uses adiabatic ramping for the electric field and laser interaction to avoid nonadiabatic coupling of phonon modes. At the end of the first pulse, we use π pulses on both ions to remove the extra phases accumulated due to the last two terms in Eq. (3). However, this spin-echo pulse does not fully correct for the residual qubit-motion entanglement because $g_m^{i,j}(|11\rangle) + g_m^{i,j}(|00\rangle) \neq g_m^{i,j}(|01\rangle) + g_m^{i,j}(|10\rangle)$. This can be compensated with one more spin-echo pulse on each ion separately. To this end, the second pulse is applied to qubit 1 and the third pulse to qubit 2 or vice versa, with the electric field switched off, see Fig. 2(a).

Gate fidelity and scalability.—We simulate the gate dynamics generated by Eq. (1) and use process fidelity to characterize its performance. For simplicity, we first ignore the contribution of the stretch mode and set ($m = \mathrm{com}$). In Fig. 2(b), we illustrate the gate mechanism using the phase space dynamics for a two-ion crystal of

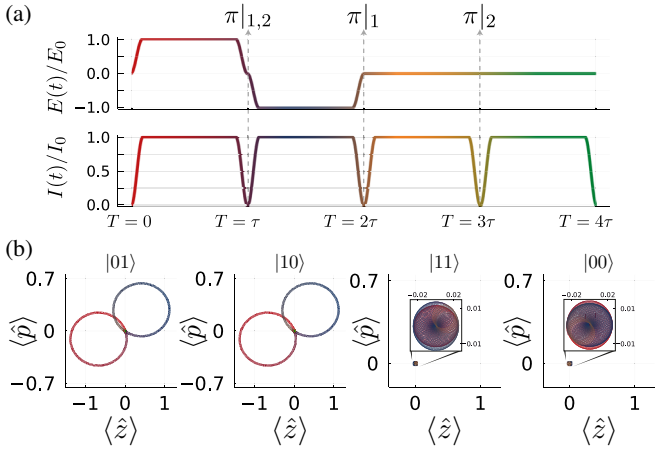

FIG. 2. (a) Pulse sequence used for the simulations; $E(t)/E_0$ and $I(t)/I_0$ are the normalized electric field and laser intensities, respectively. At the end of each of the first three pulses, we perform a π pulse on either ion 1 or 2. (b) Phase space dynamics for a two-ion crystal in natural units. When the ions are in the state $|01\rangle$ or $|10\rangle$, the electric field makes them oscillate. For the states $|11\rangle$ and $|00\rangle$, the electric field is not resonant with the c.m. mode. The residual motion of states $|11\rangle$ and $|00\rangle$ is highlighted in the insets. The parameters used are $\delta = 2\pi \times 0.001$ MHz, $E_0 = 0.269$ mV/m, $\omega_{\rm com} = 2\pi \times 1$ MHz, and $\omega_{\rm tw} = 2\pi \times 250$ kHz.

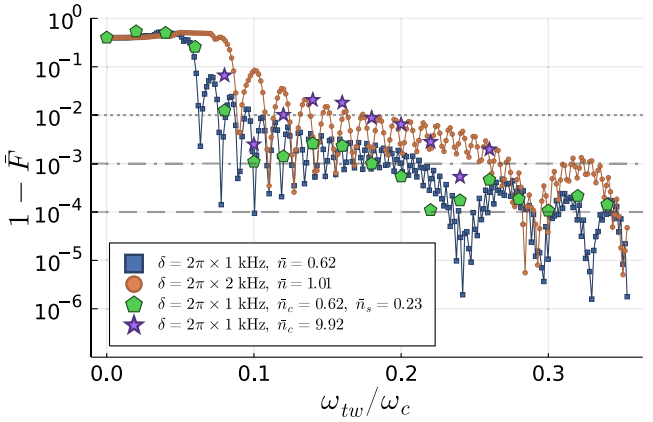

FIG. 3. Process fidelity as a function of tweezer strength for a two-ion crystal at different δ and $\bar{n}$ at $\omega_{\rm com} = 2\pi \times 1$ MHz. The resulting gate time is 4τ with $\tau = 2\pi/\delta$. The green pentagons show the fidelity for a two-ion crystal taking into account the contribution of both modes. The Fock-state cutoff for the thermal state used in the calculations is $n_{\rm max} = 20$ for the single-mode cases with $\bar{n} \leq 1$ and $n_{\rm max} = 100$ for $\bar{n} \simeq 10$. For the two modes case $n_{c,\rm max} = 14$ and $n_{s,\rm max} = 10$, with $\bar{n}_c$ and $\bar{n}_s$, respectively, the average phonon number in the c.m. and stretch mode.

$^{171}Yb^+$ prepared in the ground state of motion. For the states $|01\rangle$ and $|10\rangle$, $\hat{g}^{ij}_{\rm com} \approx 0$. Thus, these states follow the displacement generated by the electric field. On the other hand, the other two states $|11\rangle$ and $|00\rangle$ are not significantly displaced in phase space since the c.m. mode frequency is shifted by the tweezers. The chosen gate parameters ensure that the phases accumulated for these four states correspond to a geometric phase gate.

For ions initialized in a thermal state $\bar{n}$, the process fidelity is given by [16]

$$\bar{F}(\hat{U}_{\rm id}, \hat{U}_H) = \frac{\sum_l {\rm tr}[\hat{U}_{\rm id}\hat{\sigma}_l^\dagger \hat{U}_{\rm id}^\dagger \hat{\boldsymbol{\sigma}}_l(\hat{U}_H)] + d^2}{d^2(d+1)}, \qquad (4)$$

where $\hat{\boldsymbol{\sigma}}_l(\hat{U}_H) \equiv {\rm tr}_{\rm FS}(\hat{U}_{\rm tw}[|n\rangle\langle n| \otimes \hat{\sigma}_l]\hat{U}_H^\dagger)$ is the projector on one of the SU(2) d-dimensional representation of Pauli matrices (here $d = 4$ for a two-ion case) and on the Fock state $|n\rangle$, $\hat{U}_{\rm id}$ is the ideal phase gate, and $\hat{U}_H$ is the unitary generated by the Hamiltonian shown in Eq. (1) in the interaction picture.

In Fig. 3, we show the process fidelity of the proposed gate for $\delta/2\pi = 1$ kHz in the single-mode approximation with two different $\bar{n}$, along with a more thorough calculation including the stretch mode. With the single-mode approximation, shown in solid blue and dashed orange lines, $\bar{F}$ exceeds 99% at relatively low tweezer strength, $\omega_{\rm tw}/\omega_{\rm com} \gtrsim 0.1$. Fidelities higher than 99.9% can be obtained for $\omega_{\rm tw}/\omega_{\rm com} \gtrsim 0.21$. Higher tweezer intensity also allow us to perform faster gates at larger detunings while maintaining high fidelities. The green pentagons show $\bar{F}$ including the contribution of the stretch mode and confirm the validity of the single-mode approximation. We note that, when considering the contribution from both modes, we need to take into account a small correction to the electric field frequency μ. This originates from the perturbation induced by the presence of tweezers on the original eigenmodes of the system. The deviation can be calculated either by perturbation theory (two ions) or by exact diagonalization (four ions), which are shown in the second row of Table I.

We demonstrate the scalability of the scheme by considering four ions in a harmonic potential under the full tweezer Hamiltonian and including all four modes of motion. As discussed above, for each ion pair, we correct δ given the c.m. mode shift. We show that $\bar{F}$ for each ion pair at $\omega_{\rm tw} = 2\pi \times 254$ kHz, as shown in Table I, does not degrade compared to the two-ion crystal. This demonstrates the scalability of our scheme subject to laser power limitations since the required tweezer intensity $\propto N$. However, since the gate does not require the Lamb-Dicke regime, the

TABLE I. Fidelities and detunings for all combinations of pairs in a four-ion chain. All modes are in the ground state of motion, $\omega_{\rm tw} = 2\pi \times 257$ kHz and $\omega_{\rm com} = 2\pi \times 1$ MHz.

Pair	①②○○	①○③○	①○○④	○②③○
$(1-F)10^4$	3.7	4.7	2.4	1.1
$(\omega_{\rm com} - \mu)$ (kHz)	1.212	1.325	1.488	1.162

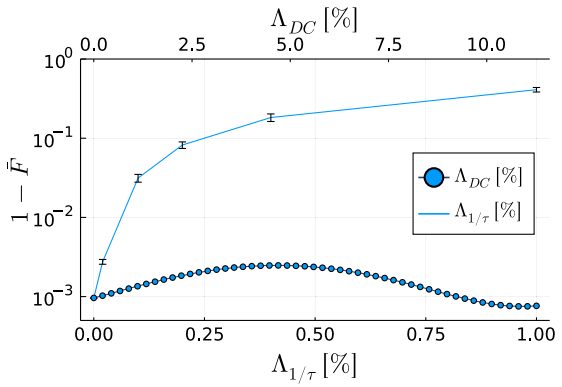

FIG. 4. Effect of noise Λ on the tweezer laser intensity at frequencies $\nu_\Lambda = 1/\tau$ and shot-to-shot noise ($\nu_\Lambda = 0$) for $\omega_{\rm tw} \sim 2\pi \times 180$ kHz, $\delta = 2\pi \times 1$ kHz, and $\omega_c = 2\pi \times 1$ MHz. The points at $\nu_\Lambda = 1/\tau$ are taken assuming a random Gaussian noise for each of the four gate pulses with a standard deviation $\sigma = \Lambda_{1/\tau}$. The points at $\nu_\Lambda = 0$ assume a change in the tweezer intensity $\Lambda_{\rm dc}$ for times longer than the gate time τ.

needed tweezer power can be limited by lowering $\omega_{\rm com}$ considerably.

Finally, we study the effect of noise Λ on the tweezer intensity during the four pulses. We consider two scenarios illustrated in Fig. 4. In $\Lambda_{\rm dc}$, we consider shot-to-shot noise at frequencies $\nu_\Lambda \ll 1/\tau$ and find that the spin-echo pulses in the gate sequence build in resilience to this type of noise (see Fig. 4). The second case is the worst case scenario: noise contribution at the same frequency as the individual laser pules ($\nu_\Lambda \sim 1/\tau$). Then the dephasing in each pulse adds up, lowering $\bar{F}$ considerably. For big ion crystals, inhomogeneities of the electric field gradient should also be considered. Our simulations indicate that these do not affect the $\bar{F}$ significantly.

Experimental considerations.—The tweezer potential takes the form $\Phi_{|j\rangle}(\mathbf{r}) \propto \alpha_{|j\rangle}(\lambda_{\rm tw}) I(\mathbf{r})$, with $\alpha_{|j\rangle}(\lambda_{\rm tw})$ as the dynamic polarizability at the tweezer wavelength $\lambda_{\rm tw}$ of qubit state $|j\rangle$ and $I(\mathbf{r})$ as the intensity pattern [17]. Expanding a Gaussian intensity pattern with waist $w_0 \gg l_m$ with $l_m = \hbar(2M\omega_m)^{-1/2}$, we obtain $\Phi_{|j\rangle}(z) \approx \Phi_{|j\rangle}(0) + M\omega_{|j\rangle}^2 z^2/2$, with $\omega_{|j\rangle}^2 = -4\Phi_{|j\rangle}(0)/(Mw_0^2)$ [17]. Here, we assumed that the tweezer has the largest curvature in the z direction and disregard the other directions.

We must identify qubit states with opposite dynamical polarizabilities such that $\omega_{|1\rangle}^2 = -\omega_{|0\rangle}^2$. Qubits encoded in the ground $S_{1/2}$ and metastable $D_{5/2}$ states of Ca^+, Sr^+, or Ba^+ fulfill this condition. The differential polarizabilities of these states can be tuned over a wide range by choosing the tweezer wavelength and Zeeman substate m_j of the $D_{5/2}$ manifold [18]. Furthermore, it is beneficial to have no residual differential Stark shift at the center of the tweezer, as this may lead to dephasing of the qubits in case of laser intensity fluctuations. The spin-echo sequence will eliminate shot-to-shot variations, but not fluctuations within a single implementation. Vanishing differential Stark shift in the center of the tweezer can be straightforwardly obtained using non-Gaussian hollow tweezers [19,20]. Another solution is to use bichromatic tweezers with wavelengths $\lambda_{\rm tw}^{(1)}$ and $\lambda_{\rm tw}^{(2)}$ and beam waists w_1 and w_2. We then require that, in the center of the tweezer ($z = 0$), $\Phi_{|0\rangle}^{(1)} + \Phi_{|0\rangle}^{(2)} = \Phi_{|1\rangle}^{(1)} + \Phi_{|1\rangle}^{(2)}$ and $\Phi_{|0\rangle}^{(1)}/w_1^2 + \Phi_{|0\rangle}^{(2)}/w_2^2 = -\Phi_{|1\rangle}^{(1)}/w_1^2 - \Phi_{|1\rangle}^{(2)}/w_2^2$. In the experimentally convenient limit where $w_1 \ll w_2$, this reduces to $\Phi_{|0\rangle}^{(1)} = -\Phi_{|1\rangle}^{(1)}$ and $\Phi_{|0\rangle}^{(2)} - \Phi_{|1\rangle}^{(2)} = 2\Phi_{|1\rangle}^{(1)}$. Note that the frequency sum and difference should not be close to any transition, as this will lead to additional Stark shifts or photon scattering.

As a practical example, we consider the qubit states $|0\rangle = |S_{1/2}, m_j = 1/2\rangle$ and $|1\rangle = |D_{5/2}, m_j = 3/2\rangle$ in $^{40}Ca^+$ [21]. We obtain $\Phi_{|0\rangle}^{(1)} = -\Phi_{|1\rangle}^{(1)}$ at around $\lambda_1 = 770$ nm [18]. The second requirement can be met by setting $\lambda_2 \approx 900$ nm. The relative close proximity of the $D_{5/2} \to P_{3/2}$ transition at 854 nm causes photon scattering $\Gamma_{\rm sc}$, which limits the attainable coupling strength. We estimate $\Gamma_{\rm sc} = \Phi_{|j\rangle}^{(i)} \Gamma_{\rm tr}/\Delta_{|j\rangle,\xi}^{(i)}$ for each transition ξ, state $|j\rangle$, and tweezer i with Γ_ξ as the transition linewidth and $\Delta_{|j\rangle,\xi}^{(i)}$ as the frequency detuning. Demanding $\Gamma_{\rm sc}/2\pi \lesssim 1\ {\rm s}^{-1}$, we find $|\Phi_{|j\rangle}^{(i)}| \lesssim 20$ MHz for all i and $|j\rangle$. This results in $|\omega_{\rm tw}| \lesssim 2\pi \times 70$ kHz for $w_2 \gg w_1 = 1\ \mu$m.

It is also possible to use qubits that are encoded in the ground $S_{1/2}$ hyperfine or Zeeman states of the ions. Here, circularly polarized tweezers may be used to obtain large differential Stark shifts. However, this approach precludes the use of magnetic field insensitive qubits [17,22]. One solution is to make use of quadrupole transitions [23,24]. These have coupling strengths that are typically $\sim 2\pi a_0/\lambda \sim 10^{-3} - 10^{-4}$ times smaller than for dipole-allowed transitions, with a_0 as the Bohr radius, but have highly suppressed photon scattering rates even at small detunings. Tuning the tweezer wavelength far away from all dipole-allowed transitions, the differential Stark shift originates from the quadrupole transitions alone [17,22,23]. In case only a single transition k' obeys $\Delta_{k'} \ll \omega_0$, with ω_0 the frequency difference between the qubit states and $\Delta_{k'}$ the detuning, we can make a two-level approximation for the transition $|0\rangle \to |k'\rangle$ and obtain $\Phi_{|0\rangle} \approx \nu_{\rm dipole} + \Omega_{k'}^2/(4\Delta_{k'})$ while $\Phi_{|1\rangle} \approx \nu_{\rm dipole}$, with $\Omega_{k'}$ as the Rabi frequency. Approximating the Stark shift due to the dipole transitions to arise mainly from a single (effective) transition, $\nu_{\rm dipole} = \Omega_{\rm dipole}^2/(4\Delta_{\rm dipole})$, we get $\Omega_{k'}^2/(4\Delta_{k'}) = -\nu_{\rm dipole}$ if we set $\Delta_{k'} = -\epsilon^2 \Delta_{\rm dipole}$ with $\Omega_{k'} = \epsilon \times \Omega_{\rm dipole}$. The detuning $\Delta_{\rm dipole}$ can be estimated as the frequency difference between the quadrupole transition and the strong $D1$ and $D2$ transitions and lies typically in the 100-THz range [25]. Therefore, we require $\Delta_{k'} \sim 1$–100 MHz for

$\epsilon = 10^{-3} - 10^{-4}$. Since we require, in addition, $\Delta_{k'} < \Omega_{k'}$ to avoid driving the transition, we get differential Stark shifts of ~0.1–10 MHz and $\omega_{\mathrm{tw}} \sim 2\pi(30\text{–}300)/\sqrt{M_u}$ kHz, with M_u as the mass of the ion in atomic mass units and $w_0 = 1$ μm. By comparison, switching to a Laguerre-Gaussian mode with radial index $p = 1$, the Rabi frequency in the center of the tweezer vanishes, whereas ω_{tw} remains unaltered for the same w_0. In this situation, we only require $\Delta_{k'} < \Omega_{k'}(z_{\mathrm{max}})$, with z_{max} as the maximum amplitude of motion of the ions during the gate. For the presented calculations $z_{\mathrm{max}} \sim 10$ nm $\ll w_0$ such that ω_{tw} can be significantly larger than for Gaussian tweezers.

Discussion.—We have proposed and analyzed a new architecture for performing quantum computation with trapped ions that uses optical tweezers and oscillating electric fields. The infrastructural simplicity of our scheme makes it attractive, while the ability to individually address the ions by the tweezer makes it universal. Furthermore, our proposal does not rely on the Lamb-Dicke approximation and is independent of the qubit separation. Residual qubit-phonon entanglement that may lead to decoherence is prevented by a spin-echo sequence. Taking experimental considerations into account, the scheme can be performed on optical qubits and on ground-state qubits. Here, either circularly polarized or hollow tweezers such as those derived from, e.g., Laguerre-Gaussian modes [19,20] could be used. The challenge will be to supply sufficient curvature to such tweezers while maintaining excellent control. For this, active stabilization of the power and direction of the tweezers may be required. Finally, it seems feasible to consider a fast gate version of the proposed gate, in analogy to Ref. [26], where electric field pulses are combined with Rydberg excitation of the trapped ions in order to implement quantum logic gates.

We gratefully acknowledge discussions with Robert Spreeuw. This work was supported by the Dutch Research Council (Grants No. 680.91.120 and No. 680.92.18.05, R. G., M. M., and R. X. S.). A. S. N. is supported by the Dutch Research Council (NWO/OCW), as part of the Quantum Software Consortium Programme (Project No. 024.003.037).

[1] J. I. Cirac, M. Lewenstein, and P. Zoller, Phys. Rev. A **51**, 1650 (1995).
[2] D. Porras and J. I. Cirac, Phys. Rev. Lett. **92**, 207901 (2004).
[3] R. Blatt and D. Wineland, Nature (London) **453**, 1008 (2008).
[4] A. H. Myerson, D. J. Szwer, S. C. Webster, D. T. C. Allcock, M. J. Curtis, G. Imreh, J. A. Sherman, D. N. Stacey, A. M. Steane, and D. M. Lucas, Phys. Rev. Lett. **100**, 200502 (2008).
[5] K. R. Brown, A. C. Wilson, Y. Colombe, C. Ospelkaus, A. M. Meier, E. Knill, D. Leibfried, and D. J. Wineland, Phys. Rev. A **84**, 030303(R) (2011).
[6] C. J. Ballance, T. P. Harty, N. M. Linke, M. A. Sepiol, and D. M. Lucas, Phys. Rev. Lett. **117**, 060504 (2016).
[7] J. P. Gaebler, T. R. Tan, Y. Lin, Y. Wan, R. Bowler, A. C. Keith, S. Glancy, K. Coakley, E. Knill, D. Leibfried, and D. J. Wineland, Phys. Rev. Lett. **117**, 060505 (2016).
[8] K. Kim, M.-S. Chang, R. Islam, S. Korenblit, L.-M. Duan, and C. Monroe, Phys. Rev. Lett. **103**, 120502 (2009).
[9] T. Olsacher, L. Postler, P. Schindler, T. Monz, P. Zoller, and L. M. Sieberer, PRX Quantum **1**, 020316 (2020).
[10] Y. H. Teoh, M. Sajjan, Z. Sun, F. Rajabi, and R. Islam, Phys. Rev. A **104**, 022420 (2021).
[11] J. D. Arias Espinoza, M. Mazzanti, K. Fouka, R. X. Schüssler, Z. Wu, P. Corboz, R. Gerritsma, and A. Safavi-Naini, Phys. Rev. A **104**, 013302 (2021).
[12] D. F. V. James, Appl. Phys. B **66**, 181 (1998).
[13] I. G. Lang and Y. A. Firsov, J. Exp. Theor. Phys. **27**, 443 (1968).
[14] A. Sørensen and K. Mølmer, Phys. Rev. Lett. **82**, 1971 (1999).
[15] D. Leibfried, B. DeMarco, V. Meyer, D. Lucas, M. Barrett, J. Britton, W. M. Itano, B. Jelenković, C. Langer, T. Rosenband, and D. J. Wineland, Nature (London) **422**, 412 (2003).
[16] M. A. Nielsen, Phys. Lett. A **303**, 249 (2002).
[17] R. Grimm, M. Weidemüller, and Y. B. Ovchinnikov, Adv. At., Mol., Opt. Phys. **42**, 95 (2000).
[18] M. Kaur, Sukhji Singh, B. K. Sahoob, and B. Arora, At. Data Nucl. Data Tables **140**, 101422 (2021).
[19] C. T. Schmiegelow, J. Schulz, H. Kaufmann, T. Ruster, U. G. Poschinger, and F. Schmidt-Kaler, Nat. Commun. **7**, 12998 (2016).
[20] M. Drechsler, S. Wolf, C. T. Schmiegelow, and F. Schmidt-Kaler, Phys. Rev. Lett. **127**, 143602 (2021).
[21] P. Schindler, D. Nigg, T. Monz, J. T. Barreiro, E. Martinez, S. X. Wang, S. Quint, M. F. Brandl, V. Nebendahl, and C. F. Roos, New J. Phys. **15**, 123012 (2013).
[22] P. J. Lee, K. A. Brickman, L. Deslauriers, P. C. Haljan, L. Duan, and C. Monroe, J. Opt. B **7**, S371 (2005).
[23] H. Häffner, S. Gulde, M. Riebe, G. Lancaster, C. Becher, J. Eschner, F. Schmidt-Kaler, and R. Blatt, Phys. Rev. Lett. **90**, 143602 (2003).
[24] L. Aolita, K. Kim, J. Benhelm, C. F. Roos, and H. Häffner, Phys. Rev. A **76**, 040303(R) (2007).
[25] NIST Atomic Spectra Database, http://physics.nist.gov/PhysRefData/ASD.
[26] J. Vogel, W. Li, A. Mokhberi, I. Lesanovsky, and F. Schmidt-Kaler, Phys. Rev. Lett. **123**, 153603 (2019).